Dyes and Pigments 204 (2022) 110390

Contents lists available at ScienceDirect

Dyes and Pigments

journal homepage: www.elsevier.com/locate/dyepig

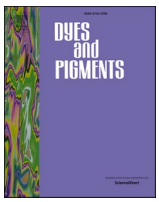

Synthesis, characterization, electrochemical, spectroelectrochemical and dye-sensitized solar cell properties of Phthalocyanines Containing Carboxylic Acid Anchoring Groups as photosensitizer

Gülnur Keser Karaoğlan [a,*], Arif Hışır [a], Yaren Erdağ Maden [b], Mücella Özbay Karakuş [c], Atıf Koca [b,**]

[a] Department of Chemistry, Yildiz Technical University, 34220, Esenler, Istanbul, Turkey
[b] Department of Chemical Engineering, Engineering Faculty, Marmara University, İstanbul, Turkey
[c] The Faculty of Engineering, Computer Engineering Department, Bozok University, Yozgat, Turkey

ARTICLE INFO

Keywords:
Phthalocyanine
Carboxylic acid
Electrochemistry
Spectroelectrochemistry
Dye sensitized solar cell

ABSTRACT

Peripherally tetra-4-carboxyethylphenoxy substituted oxotitanium (IV), cobalt(II), zinc(II) and metal free phthalocyanines were synthesized to research the sensitizing abilities of these dye molecules in standard dye-sensitized solar cells (DSSCs). All the synthesized phthalocyanine complexes have been characterized by using elemental analyses, UV–Vis, FT-IR, ^{1}H NMR and MALDI-TOF MS spectroscopic techniques. Electrochemistry of metallo phthalocyanines (MPcs) were studied with electrochemical and in-situ spectroelectrochemical measurements. H_2Pc (**7**) and ZnPc (**5**) illustrated similar Pc based electron transfer reactions. Differently, CoPc (**6**) and TiOPc (**4**) illustrated metal based redox reactions, which enhanced the redox functionality of these complexes. Metal based reductions for CoPc (**6**) and TiOPc (**4**) were recorded in addition to the Pc based one. In-situ spectroelectrochemical measurements supported the proposed voltametric mechanism. Moreover, the color and spectra of the electrogenerated species were determined with the in-situ spectroelectrochemical analyses to predict possible optoelectrochemical application of the complexes. Pronounced optical and color changes during the electrolysis of the complexes indicated electrooptical and possible solid state electrochemical functionality of the complexes. TiO_2 semiconductor on the fluoride doped indium tin oxide coated glass electrode (FTO) was decorated with H_2Pc (**7**) and TiOPc (**4**) bearing four carboxyl anchoring groups and they were first of all tested as possible dye for the DSSC. H_2Pc (**7**), TiOPc (**4**), CoPc (**6**) and ZnPc (**5**) dyes used in DSSCs showed 2.9%, 3.3%, 1.02% and 2.2% of power conversion efficiencies respectively.

1. Introduction

Metallo phthalocyanines (MPcs) find application in many electrochemical fields due to their superior redox properties. Tailoring the redox activities of MPcs are required to extent their usage in different electrochemical application areas such as electrocatalytic [1,2], electrochemical sensor [3,4] and electrochromic [5,6] fields. In addition to these applications, MPcs containing suitable anchoring substituents can also be used as functional dyes in DSSC applications. In the literature various MPcs were tested as possible dyes in DSSCs [7–10]. Intense absorption properties of MPcs in the red/near-IR (Q band) regions of the light spectrum in addition to the superior electrochemical, photochemical, and thermal stability made them suitable for the one of the best choices for the dyes in DSSCs. New studies are focused on the exploring new MPcs having efficient light absorption and good anchoring substituents for the strong interaction with the semiconductors and efficient electron transfer to the semiconductor [10,11]. Li et al. summarized phthalocyanine analogues used in DSSCs and reported the effects of the distance of the dye molecule from the surface of the semiconductor nanoparticles, the redox potentials and the directionality of the anchoring groups on the performance of the dyes [12]. In the literature, among various MPcs, while Zn^{2+} metal center has been generally preferred for peripherally or non-peripherally substituted Pcs in DSSCs [7,8,13–15], Al^{3+} and Si^{4+} metal containing Pcs are preferred

* Corresponding author.
** Corresponding author..
E-mail addresses: gkeser@yildiz.edu.tr (G.K. Karaoğlan), akoca@marmara.edu.tr (A. Koca).

https://doi.org/10.1016/j.dyepig.2022.110390
Received 21 February 2022; Received in revised form 27 April 2022; Accepted 4 May 2022
Available online 8 May 2022
0143-7208/© 2022 Elsevier Ltd. All rights reserved.

for dyes containing axial anchoring groups [10,11,16,17]. For example, García-Iglesias et al. developed an unsymmetrical ZnPc sensitizer that consists of three *tert*-butyl and two carboxylic acid groups and recorded 5.9 mA cm^{-2} of the short circuit current density (J_{sc}), 662 mV of the open-circuit voltage (V_{oc}), and 0.76 of fill factor (FF) and 2.95% of the power conversion efficiency (η) with ZnPc having one carboxylic acid groups. Whereas 7.0 mA cm^{-2} of J_{sc}, 634 mV of V_{oc}, 0.74 of ff, and 3.20% of η were obtained with ZnPc having two carboxylic acid groups [7]. This result indicated that increasing the number of anchoring groups enhanced the DSSC performance. In another recent study, Siddique et al. reported the DSSC performances of five different ZnPc substituting with various groups isopropoxy, cyano, fluoro, methoxycarbonyl, and dicyanomethyl moieties [14]. They proved that the substituents of the MPc influence the coulombic force of interaction between holes and electrons and indicated that the molecule having a low value of exciton binding energy shows low hole and electron interaction [14]. Recently, Harmandar and her coworkers reported 6.67% of η with an asymmetric zinc phthalocyanine dye bearing three 2, 6-di-*tert*-butyl-4-methylphenoxy donor groups and one carboxylic acid anchoring group [15]. Yıldız and coworkers reached to 2.04% of η with a zinc phthalocyanine complex containing six 2,6-diphenylphenoxy donor groups and one pyrazole-3-carboxylic acid anchoring group, which is better than the performance of ZnPc bearing *tert*-butyl (η = 1.74%) and hexylsulfanyl (η = 1.89%) donor groups [18]. These studies indicated that altering the number and type of the substituents and the number of anchoring groups significantly influence the DSSC performances. It is well reported that dyes, like MPcs, absorbing wide range of the spectrum, strongly binding to the surface of the semiconductors, having high redox activity and stable are preferred as the good alternatives as the dye in DSSCs [12]. Symmetrical and unsymmetrical substitution of MPcs significantly influence the DSSC performance. Urbani et al. published a review paper on the DSSC performance of MPcs, and they stated that at least tetra anchoring groups on the symmetrical MPcs enhanced the strength between MPcs and electronic coupling between the LUMO of the dye and the Ti 3d orbital. However, these type of MPcs have a strong tendency to aggregate and exist mainly as dimeric forms on the TiO2 films [19]. To solve these problems unsymmetrical substitution of MPcs have been preferred by using one or two They also stated that anchoring groups with unsymmetrical bulky groups, which prevent aggregation and increase solubility [19].

The studies indicated that MPcs generally having various anchoring groups, such as, –COOH, or $–SO_3H$, on the peripheral, non-peripheral or axial positions have possibility to give high power conversion efficiency and metal centers and substituents types and numbers carrying anchoring groups are the critical factors for the better performance, Thus here we have synthesized new MPcs having tetra –COOH anchoring group containing 4-(4- carboxyethylphenoxy) substituents at the peripheral positions of MPcs and then their detailed electrochemical and spectroelectrochemical characterizations were performed to illustrate their suitability as dyes in DSSCs. Finally, as examples, H_2Pc (**7**) and TiOPc (**4**) compounds bearing 4-(4- carboxyethylphenoxy) substituents were first of all tested in DSSCs to achieve high power conversion efficiency. Although MPcs bearing Zn^{2+}, Al^{3+}, and Si^{4+} metal centers are often preferred as dyes in DSSCs, metal free and titanyl phthalocyanines are rarely studied [20–22]. Thus, the results of this study will present the usability of these compounds in DSSCs.

2. Experimental

2.1. Instruments and chemicals

All chemicals and solvents which were purchased in high purity and all solvents were dried on molecular sieves (4A°). 4-(4-carboxyethylphenoxy) phthalonitrile (**3**) and 2,9,16,23-tetrakis(4-carboxyethylphenoxy)phthalocyaninato -zinc (II) (**6**) were synthesized and purified as given in the literatures, respectively [23] (Please refer to the Supporting Information section).

2.2. Synthesis and characterization

2.2.1. 4-(4- carboxyethylphenoxy) phthalonitrile (3)

Yield: 87% (2.54 g); m.p. 140–145 °C. FTIR υ_{max}/cm^{-1}: 2800–3287 (carboxylic acid –OH), 3072 (-CH arom.), 2990, 2835 (-CH, aliph.), 2232 (-C≡N), 1674 (C═O), 1623-1503 (C═C), 1251-1168 (Ar-O-Ar); ^{1}H NMR (d_6- DMSO) δ, ppm: 2.56 (2H, t, J = 8.75 Hz, $–CH_2$), 2.86 (2H, t, J = 8.75 Hz, $–CH_2$), 7.11 (2H, d, J = 8.5 Hz, Ar–H), 7.36–7.32 (3H, m, Ar–H), 7.75 (1H, d, J = 2.5 Hz, Ar–H), 8.08 (1H, d, J = 8.5 Hz, Ar–H), 12.15 (1H, s, carboxylic acid OH); ^{13}C NMR (125 MHz, DMSO- d_6) δ, ppm: 174.12, 161.71, 152.31, 139.03, 136.71, 130.82, 122.90, 122.11, 120.69, 117.10, 116.36, 115.84, 108.38, 35.54, 30.10 ppm; Anal. Calc. for $C_{17}H_{12}N_2O_3$ (292.069 g/mol): C, 69.86; H, 4.14; N, 9.58; found: C, 69.52; H, 4.01; N, 9.32%; MS *m/z* (100%) Calc.: 292.273; Found: 315.07 $[M+Na]^+$.

2.2.2. General procedure for the synthesis of phthalocyanine compounds (4–7)

A mixture of 4-(4-carboxyethylphenoxy)phthalonitrile (**3**) (2.92 g, 10.0 mmol), a certain amount of the proper anhydrous metal salts [except for **7**, $Ti(OCHCH_3CH_3)_4$ (0.85 g, 2.5 mmol) for **4**, $Co(AcO)_2$ (0.43 g, 2.5 mmol) for **5** or $Zn(AcO)_2$ (0.46 g, 2.5 mmol) for **6**] and a catalytic amount of DBU was stirred in 2 mL of dry DMF under argon atmosphere for 24 h at 160 °C. After cooling to room temperature, the reaction mixture was acidified with 0.1 M aqueous HCl solution, and the resulting precipitate was centrifuged, and the supernatant discarded. The precipitate was washed several times with water, ethanol, and methanol respectively. After the product was dried in vacuum the pure substance was obtained by column chromatography with silica gel by using THF: n-hexane = 3:0.5 (v/v) as eluent. The green pure compound has high solubility in acetone, DMF, $CHCl_3$, THF, and DMSO.

2.2.2.1. 2,9,16,23-tetrakis(4- carboxyethylphenoxy)phthalocyaninato -oxotitanium (IV) (4). Yield: 1.22 g (40%); m.p. > 200 °C. FT-IR (ν_{max}/cm^{-1}): 2527–3658 (carboxylic acid –OH), 3060 (-CH, arom.), 2926, 2865 (-CH, aliph.), 1716 (-C═O), 1599-1398 (-C═C-, arom.), 1223 (Ar-O-Ar); ^{1}H NMR (DMSO-d_6) δ, ppm: 7.10–8.17 (m, 28H, Ar–H), 2.54–3.01 (m, 16H, $–CH_2$); UV–Vis (DMF) λ_{max}, nm (10^{-5} log ε, L mol^{-1} cm^{-1}): 698 (5.08), 632 (4.46), 352 (4.81); Anal. Calc. $C_{68}H_{48}N_8O_{13}Ti$ (1233.02 g/mol): C, 66.24; H, 3.92; N, 9.09; Found: C, 66.32; H, 4.03; N 9.01%; MS (MALDI-TOF): *m/z* (100%) 1234.09 g/mol $[M+H]^+$, 1251.38 g/mol $[M + H_2O]^+$, 1269.41 g/mol $[M+2H_2O]^+$, 1287.33 g/mol $[M+3H_2O]^+$, 1326.79 g/mol $[M+5H_2O]^+$, 1341.43 g/mol $[M+6H_2O]^+$, 1359.24 g/mol $[M+7H_2O]^+$.

2.2.2.2. 2,9,16,23-tetrakis(4- carboxyethylphenoxy)phthalocyaninato -cobalt (II) (5). Yield: 1.07 g (35%); m.p. > 200 °C. FT-IR (ν_{max}/cm^{-1}): 2244–3276 (carboxylic acid –OH), 3027 (-CH, arom.), 2988, 2805 (-CH, aliph.), 1720 (-C═O), 1600-1401 (-C═C-, arom.), 1222 (Ar-O-Ar); UV–Vis (DMF) λ_{max}, nm (10^{-5} log ε, L mol^{-1} cm^{-1}): 665 (4.97), 604 (4.88), 335 (4.87); Anal. Calc. $C_{68}H_{48}N_8O_{12}Co$ (1228.09 g/mol): C, 66.50; H, 3.94; N, 9.12; Found: C, 66.23; H, 3.99; N 9.14%; MS (MALDI-TOF): *m/z* (100%) 1229.40 g/mol $[M+H]^+$.

2.2.2.3. 2,9,16,23-tetrakis(4- carboxyethylphenoxy)phthalocyaninato -zinc (II) (6). Yield: 1.85 g (60%); m.p. > 200 °C. FT-IR (ν_{max}/cm^{-1}): 2417–3456 (carboxylic acid –OH), 3059 (-CH, arom.), 2928, 2869 (-CH, aliph.), 1717 (-C═O), 1606-1469 (-C═C-, arom.), 1228 (Ar-O-Ar); ^{1}H NMR (DMSO-d_6) δ, ppm: 12.21 (s, 4H, carboxylic acid OH), 7.10–8.87 (m, 28H, Ar–H), 2.94–3.03 (m, 8H, $–CH_2$), 2.63–2.89 (m, 8H, $–CH_2$); UV–Vis (DMF) λ_{max}, nm (10^{-5} log ε, L mol^{-1} cm^{-1}): 678 (5.05), 615 (4.42), 357 (4.71); Anal. Calc. $C_{68}H_{48}N_8O_{12}Zn$ (1234.54 g/mol): C, 66.16; H, 3.92; N, 9.08; Found: C, 66.83; H, 3.90; N 9.16%; MS (MALDI-

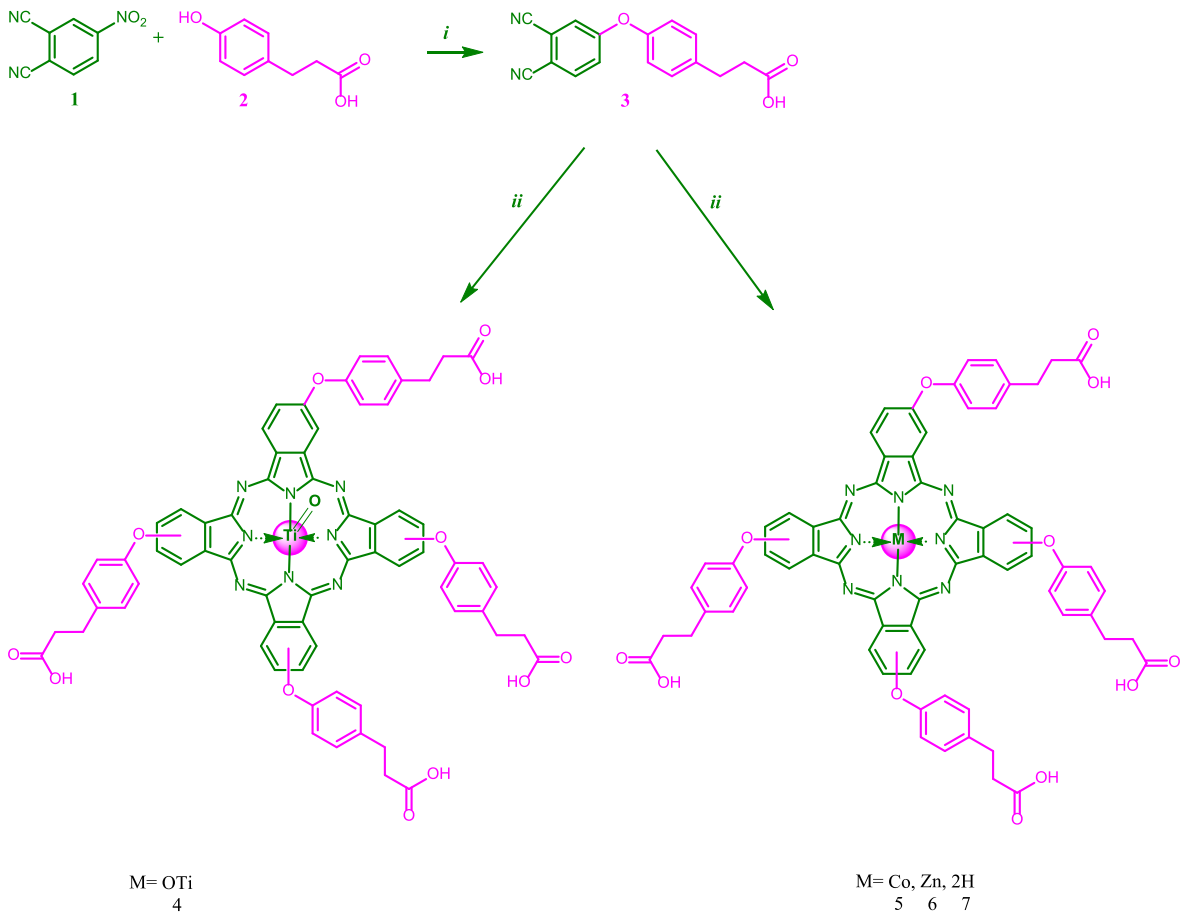

Scheme 1. The synthesis of Pcs **4**–**7**. (*i*) K_2CO_3, DMF, 75 °C; (*ii*) metal salts, DBU, DMF, 24 h and 160 °C.

TOF): *m/z* (100%) 1234.09 g/mol $[M]^+$.

2.2.2.4. 2,9,16,23-tetrakis(4- carboxyethylphenoxy)phthalocyanine (7). Yield: 1.30 g (44%); m.p. > 200 °C. FT-IR (ν_{max}/cm^{-1}): 3182 (-NH), 2414–3439 (carboxylic acid –OH), 3026 (-CH, arom.), 2943, 2830 (-CH, aliph.), 1709 (-C═O), 1596-1394 (-C═C-, arom.), 1213 (Ar-O-Ar); ^{1}H NMR (DMSO-d_6) δ, ppm: 11.25 (s, 4H, carboxylic acid OH), 7.07–8.23 (m, 28H, Ar–H), 2.52–3.14 (m, 16H, –CH_2); UV–Vis (DMF) λ_{max}, nm (10^{-5} log ε, L mol^{-1} cm^{-1}): 700 (4.99), 669 (4.99), 641 (4.76), 612 (4.68) 338 (4.90); Anal. Calc. $C_{68}H_{50}N_8O_{12}$ (1171.17 g/mol): C, 69.74; H, 4.30; N, 9.57; Found: C, 69.81; H, 4.42; N 9.62%; MS (MALDI-TOF): *m/z* (100%) 1174.11 g/mol $[M+3H]^+$.

2.3. Electrochemical and in situ spectroelectrochemical measurements

All electrochemical analysis were carried out with the cyclic voltammetric (CV) and square wave voltammetric (SWV) measurements by using a Gamry Reference 600 Potentiostat/Galvanostat in an electrochemical cell having three-electrode configuration at 25 °C by following the procedure given in the literature [24,25]. Glassy carbon (GCE), Pt wire and Ag/AgCl (containing saturated KCl solution) electrodes were used as working, counter and reference electrode respectively in dichloromethane (DCM) or dimethyl sulphoxide (DMSO)/tetra butyl ammonium perchlorate (TBAP) electrolyte. *In situ* Spectroelectrochemical (SEC) and in-situ spectrochronocoulometric (SCC) measurements were carried out in homemade quartz cell by using a Reference 600 Gamry potentiostat and OceanOptics QE65000 diode array spectrophotometer (QE65000). A Pt tulle working, a platinum wire counter and silver-silver chloride (Ag/AgCl) reference electrodes were used for the *SEC* measurements.

2.4. DSSC measurements

TCO22-15 fluorine-doped tin oxide coated glasses, TiO_2 paste (Ti-Nanoxide D/SP), platisol T/SP, Iodolyte AN-50, Chenodeoxycholic Acid (CDCA) and Ruthenizer 535-bisTBA (N719) were supplied from Solaronix and $TiCl_4$ was supplied from Sigma Aldrich. The surface of TCO22-15 glasses was cleaned and TiO_2 paste was coated onto the FTO plates by the doctor-blade technique on an active square area of 0.25 cm^2 (5 × 5 mm^2) and sintered at 450 °C for 30 min 40 mM $TiCl_4$ aqueous solution was used for treatment of TiO_2 photo anode at 70 °C for 30 min. Then the TiO_2 photo anodes were sintered at 450 °C for 30 min again. When the electrodes were cooled in approximately 50 °C after the sintering procedure they were immersed in the 0.4 mM TiOPc (4), CoPc (5), ZnPc (6), and H_2Pc (7) dye solutions that prepared in dichloromethane with 10-fold chenodeoxycholic Acid (CDCA) for 18 h at room temperature.

Pre-drilled TCO22-15 glasses were coated with platisol T/SP platinum paste and sintered at 420 °C for 15 min to prepare the counter electrodes. Then the counter electrodes were sandwiched with photo electrodes by using Meltonix 1170-60 (Solaronix) 60 μm thick hot-melt sealing and Iodolyte AN-50 liquid electrolyte was syringed between two electrodes. Three samples were fabricated for each experiment to reproducibility of the experiments and to minimize the experimental errors for the solar cell measurements.

3. Results and discussions

3.1. Synthesis and characterization

The complexes (**4**–**7**) were synthesized as outlined in Scheme 1, starting from the synthesis of the phthalonitrile derivatives, namely 4-

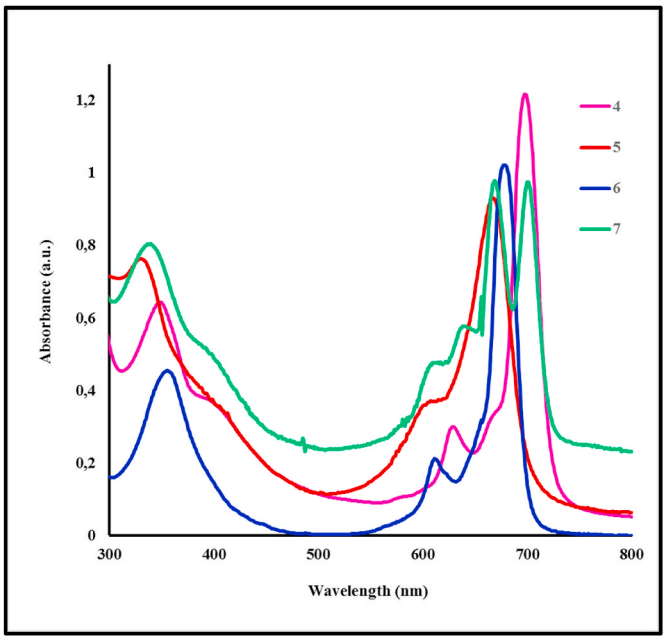

Fig. 1. UV–Vis spectra of the phthalocyanines (**4**–**7**) in DMF.

(4-carboxyethylphenoxy) phthalonitrile (**3**). The compounds **4**–**6** were synthesized by heating **4** with anhydrous $Ti(OCHCH_3CH_3)_4$, $Co(AcO)_2$ and $Zn(OAc)_2$ salts, respectively at 160 °C in a sealed tube under argon atmosphere in 40%, 35% and 60% yields, respectively (Scheme 1). Cyclotetramerization of the phthalonitrile derivative **3** to the metal-free Pc **7** was accomplished in anhydrous dimethyl formamide (DMF) at 160 °C in 44% yields, respectively (Scheme 1). Compounds **4**–**7** were synthesized in the presence of DBU as a strong base.

The structures of **4**–**7** were verified by FT-IR, UV–Vis, ^{1}H NMR and MALDI-TOF MS spectroscopic methods, as well as by elemental analysis. The ^{1}H NMR measurement of **5** was excluded due to its paramagnetic property. All the analytical and spectral data are consistent with the predicted structures. The presence of carboxylic acid groups in the metallo and metal free Pc complexes was confirmed by FT-IR spectra [23]. In the FT-IR spectrum of phthalocyanine compounds **4**–**7**, carboxylic acid –OH groups were observed in the range of 2244–3658 cm^{-1} and –C═O groups were appeared at 1716, 1720, 1717 and 1709 cm^{-1}, respectively. The missing peak of –C≡N at 2232 cm^{-1} in the FT-IR spectrum of **3** is the sign of formation of all the phthalocyanine complexes (**4**–**7**). The aromatic peaks were observed above just 3000 cm^{-1} while aliphatic peaks were showed just below 3000 cm^{-1}. The IR spectra

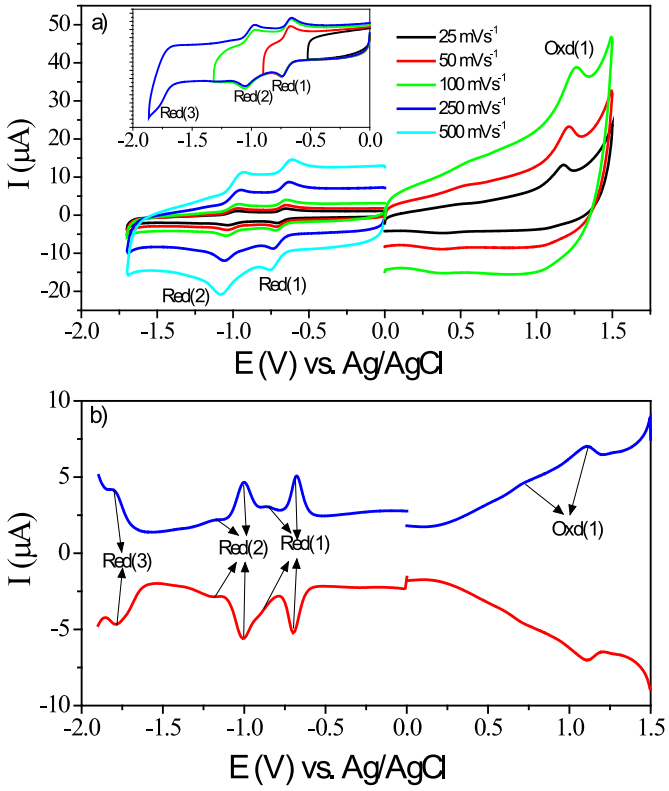

Fig. 2. CVs and SWVs of H_2Pc (**7**) (5.0×10^{-4} mol dm^{-3}) recorded at various scan rates on a GCE working electrode in DMSO/TBAP.

of compounds **4**–**7** were appeared Ar–O–Ar peaks at 1213-1228 cm^{-1}, aromatic C═C peaks at 1606-1394 cm^{-1}. The IR spectra of the Pcs **4**–**7** are very similar, with the exception of the metal-free **7** showing an NH stretching band peaks at 3182 cm^{-1} due to the inner core.

The electronic absorption spectra of the newly synthesized metallophthalocyanines **4**–**6** in DMF showed characteristic absorptions between 665 and 698 nm in the Q-band region (Fig. 1). The Q band observed for the compounds was attributed to the π/π* transition from the highest occupied molecular orbital (HOMO) to the lowest unoccupied molecular orbital (LUMO) of the Pc ring. B (or Soret) bands in the UV region at 335–357 nm were observed due to the transitions from the deeper π levels to the LUMO [23,26,27]. The split Q band of **7**, which are quite typical for metal-free Pc, showed two intense absorptions at 700, 669 nm indicating the lower symmetry (D_{2h}) of the compound (Fig. 1) [28,29].

Table 1
Electrochemical data of the complexes in DMSO/TBAP solution. All potentials were given versus Ag/AgCl.

Complexes	$E_{1/2}$ (V) of Redox Processes									
	Red(1)	Red(2)	Red(3)	Red(4)	Oxd(1)	Oxd(2)	[b]E_{LUMO}	[c]E_{HOMO}	E_{gap} (eV)	Ref.
TiOPc(4)[a]	−0.43	−0.58	−0.80	−0.94	0.56	0.98	−3.90	−4.89	0.99	tw
CoPc(5)	−0.41	−1.28	−1.87	–	0.19	0.89 (1.04)	−3.92	−4.52	0.60	tw
ZnPc(6)	−0.86	−1.10	–	–	0.76 (0.62)	0.96	−3.47	−4.95	1.48	tw
H_2Pc(7)	−0.70	−1.01	−1.77		1.10 (0.70)	–	−3.63	−5,.03	1.40	tw
CoPc	−0.48	−1.29	−1.92		0.30	0.91				[36]
MnClPc	−0.30	−0.90	−1.36		0.38 (0.51)	0.88				[36]
CuPc(mpt)	−0.95	−1.21	−1.88		0.58	1.30				[30]
CoPc(t-SA)	−0.62	−0.95	−1.63		0.67	0.89				[46]
CoTMPyrPc	−0.50	−1.34	−1.93		0.47	1.00				[58]
MnTMPyrPc	−0.06	−0.68	−1.19		–	–				[58]
MnClPc(m)	−0.23	−0.80	−1.04		–	–				[59]

[a] TiOPc(4) illustrated 5., 6. and 7. reduction processes at −1.33, −1.62, and −2.01 V respectively.
[b] E_{HOMO} = -4.78 +($E_{1/2}$ (Fc)-$E_{1/2}$ (Oxd(1)).
[c] E_{LUMO} = -4.78 +($E_{1/2}$ (Fc)-$E_{1/2}$ (Red(1)).

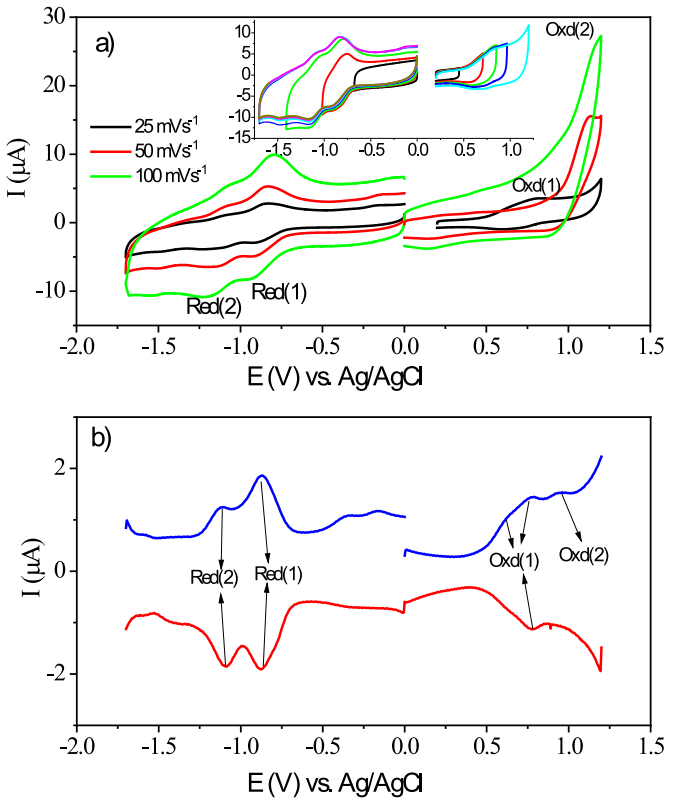

Fig. 3. a) CVs (inset: CVs recorded with various vertex potentials at 100 mVs^{-1}) and **b**) SWVs of ZnPc (**6**) (5.0×10^{-4} mol dm^{-3}) recorded at various scan rates on a GCE working electrode in DMSO/TBAP.

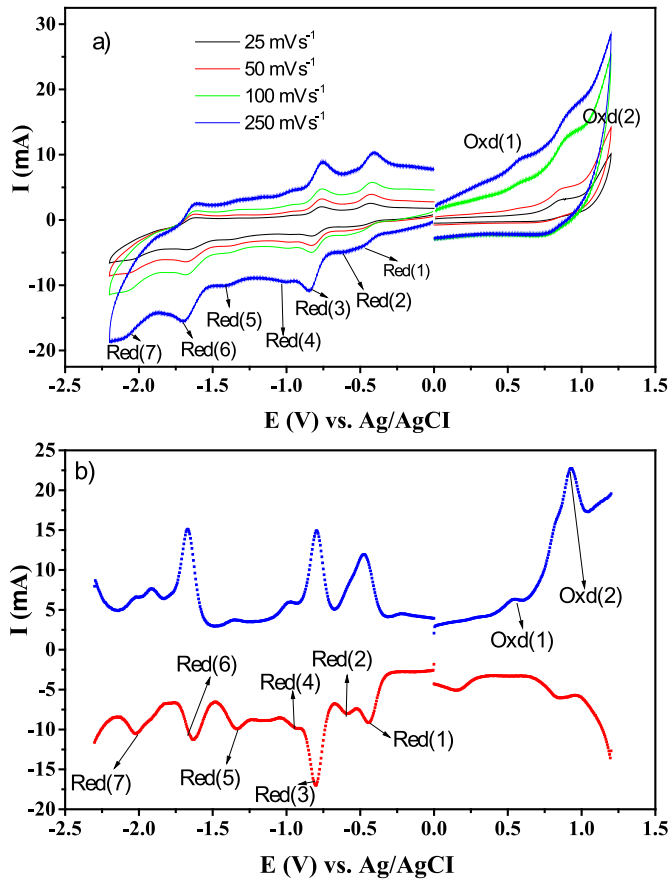

Fig. 4. CVs and SWVs of TiOPc (**4**) (5.0×10^{-4} mol dm^{-3}) recorded at various scan rates on a GCE working electrode in DMSO/TBAP.

^{1}H NMR spectra were also in accordance with the structures of the synthesized compounds. ^{1}H NMR measurements were precluded, due to its paramagnetic nature for **5**. ^{1}H NMR spectra of **6** and **7** in deuterated dimethyl sulphoxide gave a singlet at δ 12.21 and 11.25 ppm (COOH), respectively. The aromatic protons appeared between δ 7.07–8.87 ppm for **4**, **6** and **7** while the aliphatic protons were observed in the range δ 2.52–3.14 ppm for **4**, **6** and **7**.

In the mass spectrum of compounds **5**, **6** and **7** the presence of molecular ion peaks at $m/z = 1229.40$ $[M+H]^+$, 1234.09 $[M]^+$ and 1174.11 $[M+3H]^+$ respectively, clearly indicates the formation of desired products. In the case of **4** the highest values observed in the spectrum correspond to fragment ions 1234.09 $[M+H]^+$, 1251.38 $[M + H_2O]^+$, 1269.41 $[M+2H_2O]^+$, 1287.33 $[M+3H_2O]^+$, 1326.79 $[M+5H_2O]^+$, 1341.43 $[M+6H_2O]^+$ and 1359.24 $[M+7H_2O]^+$.

3.2. Voltammetric measurements

Voltammograms of MPcs having 4-(4- carboxyethylphenoxy) substituents were recorded on GCE in DCM and/or DMSO/TBAP electrolyte and the half wave peak potentials ($E_{1/2}$) derived the voltammograms are tabulated in Table 1 for the comparison. As depicted in Table 1, MPcs having redox inactive metal centers such as H^+ and Zn^{2+}, illustrate only Pc based redox responses, there is no doubt on the redox mechanism of these complexes since the redox inactivity of the metal center and substituents. Voltammetric results of H_2Pc (**7**) and ZnPc (**6**) are given in Fig. 2 and Fig. 3 as examples. During the negative potential scans, two quasi reversible redox couples of H_2Pc (**7**) are observed at −0.70 V (Red (1)), −1.01 V (Red(2)). Third reduction process could be recorded with SWV at −177 V as shown in Fig. 2b. Moreover, an irreversible oxidation process which is split into two waves, is also observed at 0.70 and 1.10 V (Oxd(1)). The small wave clearly observed with SWV may be due to the electron transfer reaction of the aggregated species. The redox positions and general behaviors of them are in consistence with the similar H_2Pcs reported in the literature. Due to the different electron releasing/withdrawing nature of the substituents, the redox coupes of H_2Pc (**7**) are slightly shift towards the positive potentials.

As shown in the CVs and SWVs of ZnPc (**6**), two reduction and two oxidation couples are observed at −0.86 V (Red(1)), −1.10 V (Red(2)), 0.76 V (Oxd(1)), and 0.96 V (Oxd(2)) respectively (Fig. 3).A small oxidation wave is observed at 0.62 V due to the oxidation of the aggregated species. Moreover, due to the aggregation of the complex, small waves just after the first and second reduction reactions are observed (in the SWVs), which are assigned to the reduction of the aggregated species. When compared with the similar ZnPc reported in the literature [30–33], all redox couples are assigned to the electron transfer reaction of the Pc ring. With respect to peak to peak separation (ΔE_p), and peak current ratio (I_{pa}/I_{pc}), while the Red(1) and Red(2) are electrochemically and chemically reversible, the other processes are chemically irreversible.

Changing the metal center of Pc ring with Co^{+2} and $Ti^{+4}O$ cations, considerably enhanced the redox richness as shown in Figs. 4–6. TiOPc (**4**) shows completely different voltammograms than those of ZnPc (**6**) and H_2Pc (**7**), due to the redox activity of the $Ti^{+4}O$ metal center as shown in Figs. 4 and 5. Totally seven reduction and two oxidation processes are recorded during the cathodic and anodic potential scans respectively. When the redox responses of TiOPc (**4**) are compared with the similar TiOPc in the literature, the redox mechanism given in Eq. (1)–(9) can be easily proposed. In the literature, most of the electrochemistry of TiOPc (**4**) are reported by Koca et al. [34–37]. In all these studies, metal-ligand-metal-ligand redox assignments are proposed for the first fourth reduction processes. Similar redox mechanism was reported by Bıyıklıoğlu. and [38–40] and Arslanoğlu et al. [41]. However,

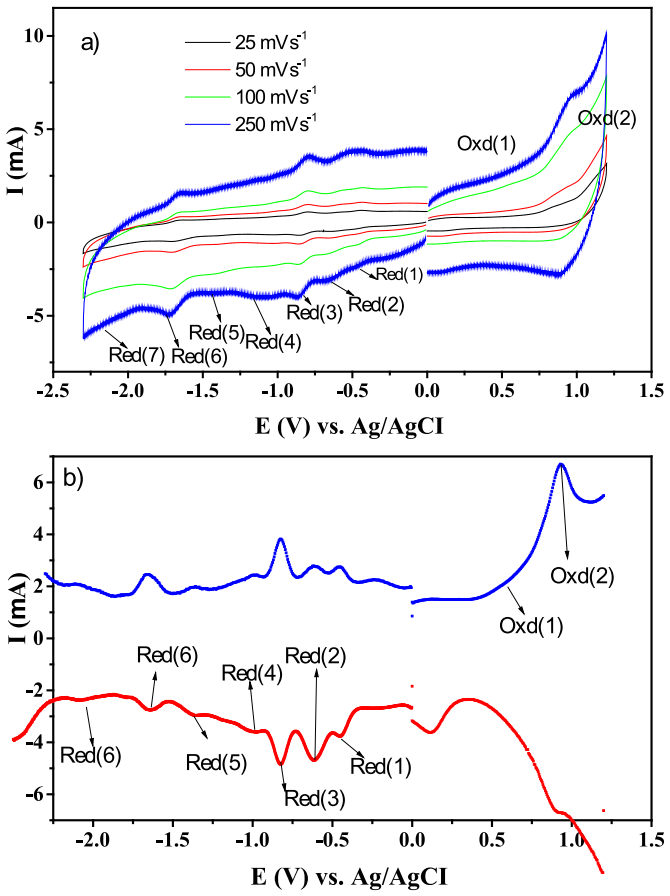

Fig. 5. CVs and SWVs of TiOPc (**4**) (1.0×10^{-4} mol dm^{-3}) recorded at various scan rates on a GCE working electrode in DMSO/TBAP.

He et al. differently reported two-electron metal-ligand and two-electron metal ligand processes [42]. A different redox mechanism was proposed by Nyokong research group [43–45]. In their studies, overlap of voltammograms for two 1-electron reductions resulted in one couple for the $[Ti^{IV}OPc^{2-}]/[Ti^{II}OPc^{2-}]^{2-}$ and $[Ti^{II}OPc^{2-}]^{2-}/[Ti^{I}OPc^{3-}]^{4-}$ processes. These studies indicate that the metal and Pc based process can be recorded separately or overlap in a single wave. In this study, all of the 1-electron reduction reactions of TiOPc (**4**) can be clearly recorded especially with SWVs as shown Figs. 4 and 5. When compared with the well documented studies, the first four reduction processes can be easily assigned to the metal-ligand-metal-ligand processes. The concentration of the solutions significantly influences the peak current ration of metal and Pc based processes. As shown in the SWV of the complex, the Red (1) wave has higher current than Red (2) wave in the concentrated solution (Fig. 4b). However, Red (2) wave get higher current in the diluted solution (Fig. 5b). Although the redox processes have different peak current, the controlled potential coulometric analysis performed at −1.20 V indicated one-electron transfer character of each redox process. These responses most probably resulted from the aggregation of the complex in the concentrated solution, which make difficult to the reduction of the central metal ion.

$$[Ti^{III}OPc^{1-}]^{1+} - e^- \xleftrightarrow{E_{1/2}=0.98\ V\ (Oxd(2))} [Ti^{III}OPc^{0}]^{2+} \quad (1)$$

$$[Ti^{IV}OPc^{2-}] - e^- \xleftrightarrow{E_{1/2}=0.56\ V\ (Oxd(1))} [Ti^{III}OPc^{1-}]^{1+} \quad (2)$$

$$[Ti^{IV}OPc^{2-}] + e^- \xleftrightarrow{E_{1/2}=-0.43\ V\ (Red(1))} [Ti^{III}OPc^{2-}]^{1-} \quad (3)$$

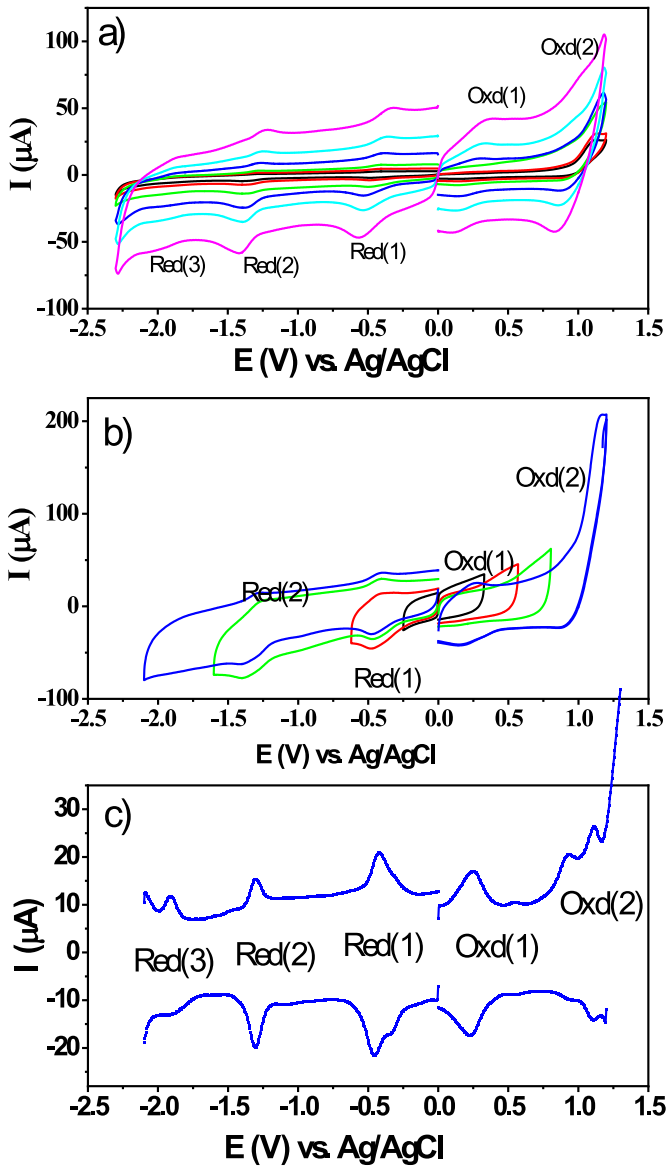

Fig. 6. CVs and SWVs of CoPc (**5**) (5.0×10^{-4} mol dm^{-3}) recorded at various scan rates on a GCE working electrode in DMSO/TBAP.

$$[Ti^{III}OPc^{2-}]^{1-} + e^- \xleftrightarrow{E_{1/2}=-0.58\ V\ (Red(2))} [Ti^{III}OPc^{3-}]^{2-} \quad (4)$$

$$[Ti^{III}OPc^{3-}]^{2-} + e^- \xleftrightarrow{E_{1/2}=-0.80\ V\ (Red(3))} [Ti^{II}OPc^{3-}]^{3-} \quad (5)$$

$$[Ti^{II}OPc^{3-}]^{3-} + e^- \xleftrightarrow{E_{1/2}=-0.94\ V(Red(4))} [Ti^{II}OPc^{4-}]^{4-} \quad (6)$$

$$[Ti^{II}OPc^{4-}]^{4-} + e^- \xleftrightarrow{E_{1/2}=-1.33\ V\ (Red(5))} [Ti^{I}OPc^{4-}]^{5-} \quad (7)$$

$$[Ti^{I}OPc^{4-}]^{5-} + e^- \xleftrightarrow{E_{1/2}=-1.62\ V\ (Red(6))} [Ti^{I}OPc^{5-}]^{6-} \quad (8)$$

$$[Ti^{I}OPc^{5-}]^{6-} + e^- \xleftrightarrow{E_{1/2}=-2.01\ V\ (Red(7))} [Ti^{I}OPc^{6-}]^{7-} \quad (9)$$

In order to investigate influences of using Co^{2+} metal center, redox properties of CoPc (**5**) are represented in Fig. 6. In the literature, numerous CoPc having various substituents were published and it has been reported that the substituent environment does not influence

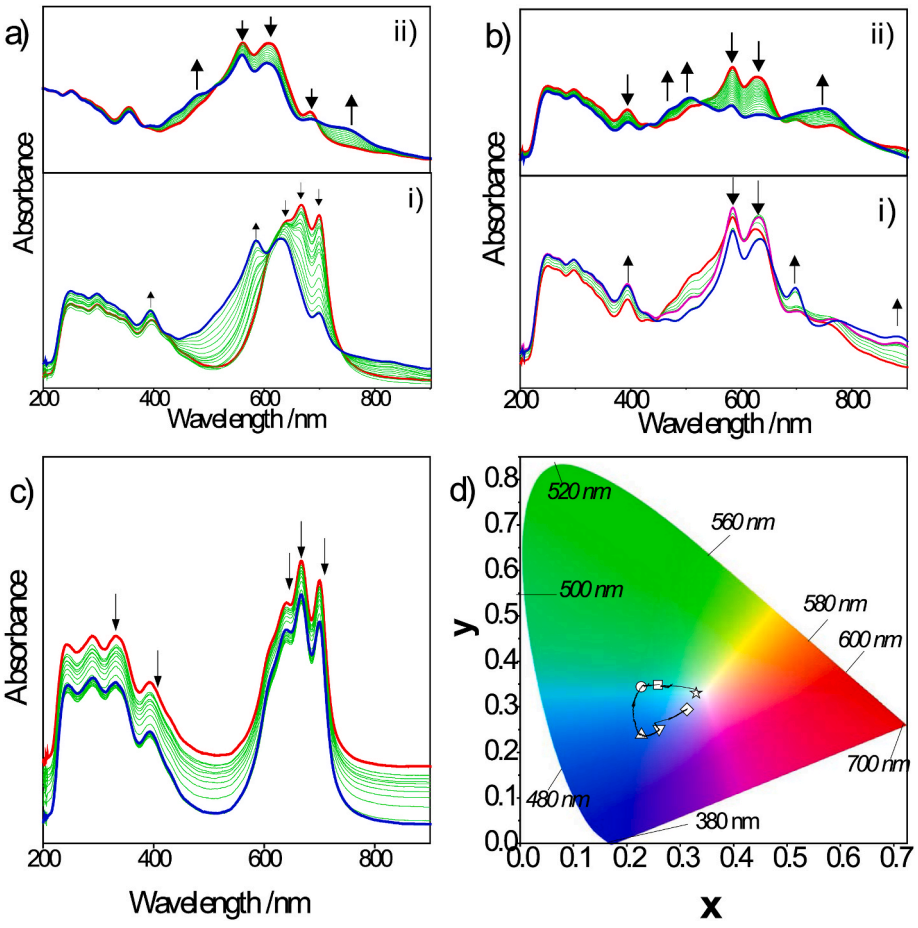

Fig. 7. In-situ UV–Vis spectral changes of H_2Pc (**7**) in DMSO/TBAP electrolyte. **a**) i: $E_{app} = -0.50$ V, ii: $E_{app} = -0.70$ V, **b**) i: $E_{app} = -0.90$ V and then ii: 1.00 V, **c**) $E_{app} = 0.40$ V and then 1.00 V, **d**) Chromaticity diagram (each symbol represents the color of electro-generated species; □: $[Ti^{IV}OPc^{2-}]$; ○: $[Ti^{III}OPc^{2-}]^{1-}$; △: $[Ti^{III}OPc^{3-}]^{2-}$; ▽: $[Ti^{II}OPc^{3-}]^{3-}$; ☆: $[Ti^{IV}OPc^{1-}]^{1+}$.

electrochemical mechanism but influence the peak positions and reversibility of the process. In these studies, metal-ligand-ligand reduction and metal-ligand-ligand based oxidation mechanism were reported in polar coordinating electrolyte [46–50]. Similarly here, CoPc (**5**) illustrates three reduction and two oxidation couples at −0.41 V (Red(1)), −1.28 V (Red(2)), −1.87 V (Red(3), 0.19 V (Oxd(1)), and 0.89 V Oxd(2)), which are assigned to metal-ligand based reduction and metal-ligand based oxidation processes [33,46,51,52]. The proposed mechanism for these complexes is proved with the in situ spectroelectrochemical measurements discussed below.

3.3. *In-situ spectroelectrochemical measurements*

There is not a doubt on the peak assignments of H_2Pc (**7**) and ZnPc (**6**) compounds since H^+ and Zn^{2+} central cations on these molecules are redox inactive. Thus in-situ spectroelectrochemical characterizations of H_2Pc (**7**) is given in Fig. 7 as an example. Under open circuit potential, H_2Pc (**7**) illustrates common split Q bands at 666 and 689 nm and the B bands at 294 and 395 nm. During the electrolysis at the first reduction reaction potential, the split Q bands disappear, and a new Q band is obtained at 633 nm (Fig. 7a–i). Moreover, a charge transfer band is recorded at 585 nm. These spectral changes are characteristic changes for the Pc based reduction of H_2Pc (**7**) compounds. Fig. 7a–ii shows the spectral changes during the second Pc based reduction reaction of H_2Pc (**7**). While the Q band at 633 nm and the band at 585 nm decrease in intensity and a new charge transfer bands are observed at 506 and 785 nm. The observed spectral changes during the Red(3) and Red(4) processes are also consistence with the characteristic spectral changes of H_2Pc compounds in the literature (Fig. 7b i-ii). During the oxidation reaction, the oxidized cationic H_2Pc (**7**) species decompose which reflected with the decreasing of all bands as shown in Fig. 7c. Color of the compound significantly change as shown in the chromaticity diagram of the compound (Fig. 7d). The spectroelectrochemical results of the compounds indicate its functionality in various optoelectrochemical applications, such as electrochromic, photoelectrochemical and solar cell applications.

Redox activity of the central cations of TiOPc (**4**) and CoPc (**5**) complexes considerably alter the spectral changes due to the additional redox waves of $Ti^{4+}O$ and Co^{2+} ions. Spectral changes during the redox processes of TiOPc (**4**) are illustrated in Fig. 8. Slight shifting of the Q band towards the shorter wavelengths (from 700 to 690 nm) with the decrease in the intensity and decrease of the bands at 400 and 450 nm are characteristic chances for the $[Ti^{IV}OPc^{2-}]$/ $[Ti^{III}OPc^{2-}]^{1-}$ assignment for Red(1) couple of the TiOPc (Fig. 8a–i) [37,44,53]. During the Red(2) process, the Q band decrease without a shift while a new band is observed at 500 nm, which supports the occurring of $[Ti^{III}OPc^{2-}]^{1-}$/ $[Ti^{III}OPc^{3-}]^{2-}$ reduction (Fig. 8a–ii). Similarly, while the Q band shift from 690 nm to 650 nm with decreasing the band at 520 nm increases in intensity due to the reduction of $[Ti^{III}OPc^{3-}]^{2-}$ to $[Ti^{II}OPc^{3-}]^{3-}$ (Fig. 8b–i). Similarly, the spectral changes in Fig. 8b–ii are characteristic changes for the further Pc based reduction of $[Ti^{II}OPc^{3-}]^{3-}$ to $[Ti^{II}OPc^{4-}]^{4-}$. During the further reduction processes, a distinct spectral change could not be recorded due to the instability of the multi-anionic forms of the reduced species. During the oxidation reactions, all bands decreased in intensity without a shift due to the ligand-based oxidations

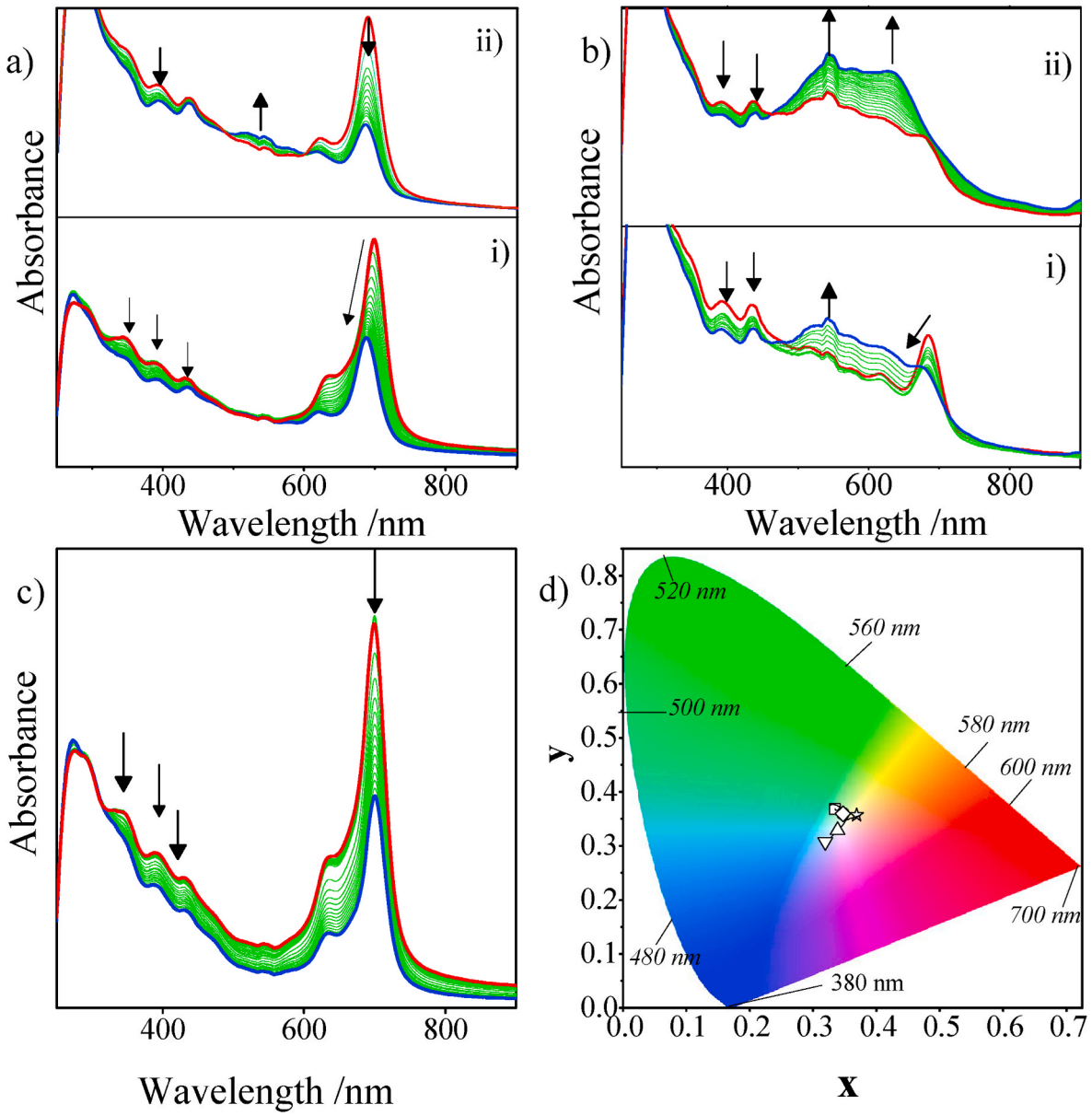

Fig. 8. In-situ UV–Vis spectral changes of TiOPc **(4)** in DMSO/TBAP electrolyte. **a**) i: $E_{app} = -0.50$ V, ii: $E_{app} = -0.70$ V, **b**) i: $E_{app} = -0.90$ V and then ii: 1.00 V, **c**) $E_{app} = 0.40$ V and then 1.00 V, **d**) Chromaticity diagram (each symbol represents the color of electro-generated species; □: $[Ti^{IV}OPc^{2-}]$; ○: $[Ti^{III}OPc^{2-}]^{1-}$; △: $[Ti^{III}OPc^{3-}]^{2-}$; ▽: $[Ti^{II}OPc^{3-}]^{3-}$; ☆: $[Ti^{IV}OPc^{1-}]^{1+}$.

and decomposition of the oxidized species (Fig. 8c). As represented in Fig. 8d, color changes from green to yellow, cyan and then blue color respectively during the reduction reactions. Similarly orange color is recorded after the oxidation reactions. The distinct color changes and multielectron redox reactions of the complex indicate its possible usage in display technologies as an electrochromic material.

In situ spectroelectrochemical response of CoPc (**5**) represented in Fig. 9 supports the assignments performed with voltametric measurements. The shifting of the Q band during the first reduction and first oxidation processes (Fig. 9a and c) supported the metal based electron transfer characters of these couples [24,49,53,54]. During the Pc based reduction, the Q bands decreased in intensity without a shift and a new band is observed in the ligand to metal charge transfer region as shown in Fig. 9b. Possible electrochromic functionality of CoPc (**5**) is shown in the chromaticity diagram (Fig. 9d). As shown in this figure each redox species of the complex has different colors, which is the desired feature for the polyelectrochromic applications.

3.4. Photovoltaic properties

In order to determine suitability of the TiOPc (4), CoPc (5), ZnPc (6), and H_2Pc (7) as dyes in DSSC, their highest occupied molecular orbital level (HOMO) and lowest unoccupied molecular orbital level (LUMO) of dyes were calculated from oxidation and reduction processes recorded with CV and SWV analyses. The E_{HOMO} and E_{LUMO} values determined are given in Table 1. In DSSCs, the LUMO energy level of Pc should be more negative than the conductivity band of TiO_2 (−4.00 eV) and the HOMO energy level should be more positive than the redox potential of the electrolyte (−4.75 eV for I^-/I^{3-}). As shown in Table 1, the HOMO and LUMO energy levels of MPcs (except CoPc (5)) are suitable for the continuous charge carrier mobility of the DSSCs to operate easily. Although LUMO energy levels of CoPc (5) seems as unsuitable, a reasonable high photovoltaic performance is also recorded with CoPc (6). These extraordinary responses may be due to the variation of the energy levels in different media. It is well known that CoPc (5)

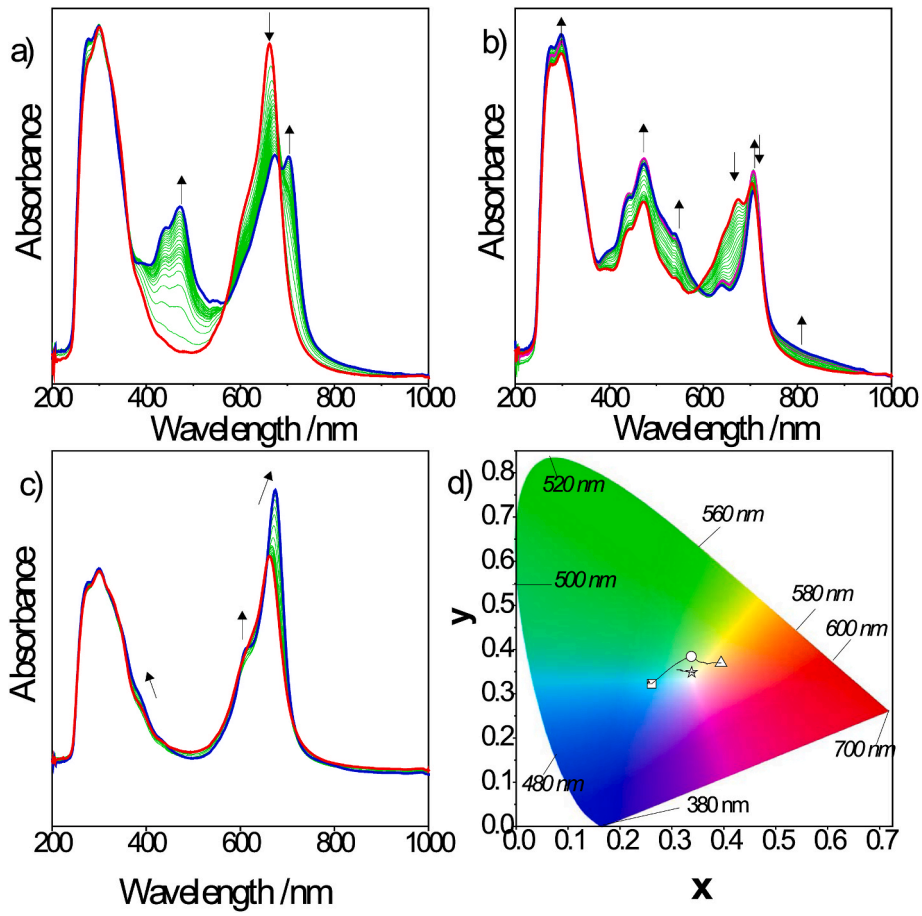

Fig. 9. In-situ UV–Vis spectral changes of CoPc (**5**) in DMSO/TBAP electrolyte. **a**) $E_{app} = -0.50$ V **b**) $E_{app} = -1.40$ V, **c**) $E_{app} = 0.50$ V, **d**) Chromaticity diagram (each symbol represents the color of electro-generated species; □: $[Co^{II}Pc^{-2}]$; ○:$[Co^{I}Pc^{-2}]^{1-}$; △: $[Co^{II}Pc^{-3}]^{2-}$; ☆: $[Co^{III}Pc^{-2}]^{1+}$.

Table 2
Photovoltaic properties of the MPc bearing DSSCs.

Dye	J_{SC} (mA/cm^2)	V_{OC} (mV)	FF (%)	η (%)	Ref.
TcZnPc1	1.05	540	70.8	0.4	[60]
4-HBa-ZnPc	6.82	860	51	2.99	[61]
4-HBa-CoPc	8.40	910	48	3.70	[61]
PCH001	6.5	635	74.3	3.05	[62]
Co-Pc-dg	5.77	740	53	2.26	[56]
Co-Pc-dp	5.28	730	52	2.01	[56]
TT1	7.60	617	75	3.52	[63]
TT2	0.90	550	72	0.4	[63]
TT3	4.80	610	74	2.20	[63]
TT4	1.44	611	75	0.67	[63]
TT5	6.80	613	74	3.10	[63]
H2TCPc	0.466	441	52	0.43	[64]
CoTCPc	0.444	281.25	47	0.23	[64]
ZnTCPc	0.555	375	45	0.37	[64]
ZnTSPc	0.466	486.75	55	0.50	[64]
TiOPc(4)	**11.72**	**466**	**60.8**	**3.32**	**tw**
CoPc (5)	**8.47**	**370**	**11.6**	**1.02**	**tw**
ZnPc (6)	**9.36**	**428**	**24.4**	**2.20**	**tw**
H_2Pc(7)	**10.98**	**471**	**56.4**	**2.92**	**tw**
N719	**19.10**	**721**	**66.4**	**9.14**	**tw**

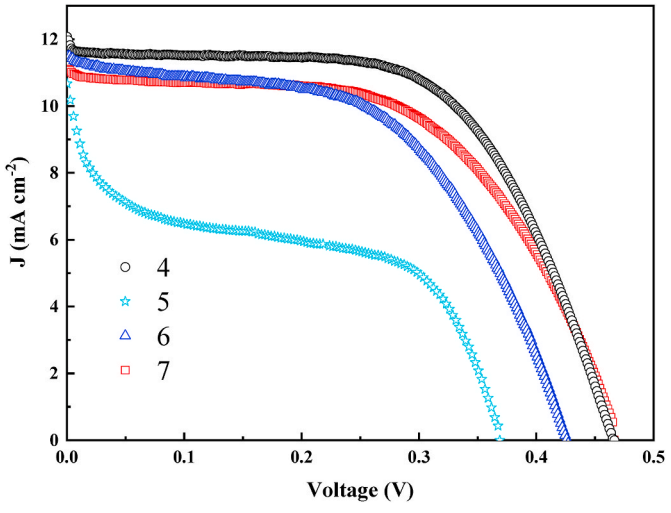

Fig. 10. J–V measurements of the DSSCs based on TiOPc (**4**), CoPc (**5**), ZnPc (**6**), and H_2Pc (**7**).

illustrated a metal based oxidation process at 0.19 V due to the stabilization of Co^{II}/Co^{III} redox couple in polar and coordinating DMSO electrolyte. However in acetonitrile this peak is not fovarable, thus the oxidation potential may shift to more positive potentials, which makes the LUMO of the complex as suitable for the continuous charge carrier mobility. The photovoltaic performances of solar cells which were constructed by using TiOPc (4), CoPc (5), ZnPc (6), and H_2Pc (7) are summarized in Table 2. As shown in this table, photovoltaic performances of H_2Pc (**7**) and TiOPc (**4**) are considerably higher than those of CoPc (5) and ZnPc (6) and they are among the MPcs having higher performances. Although high efficiency and fill factor values are obtained, the open circuit potentials of these compounds are less than the similar MPcs in the literature. The low open circuit potentials were most probably due to the shorter electron lifetime as a result of the small

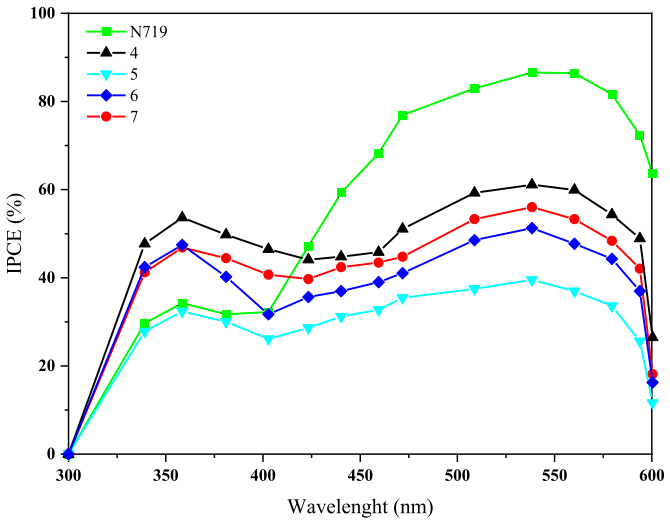

Fig. 11. IPCE plots of the DSSCs based on TiOPc (**4**), CoPc (**5**), ZnPc (**6**), H_2Pc (**7**), and N719.

blocking effect against the approach of acceptor species, which may be resulted from the low amount of adsorbed dye. The low number of adsorbed dyes may be related to the nonspherical large structure of the dyes, which makes it difficult to cover the TiO_2 surface [54]. While ZnPcs are more preferred in the literature, CoPc (5), metal free (H_2Pc (**7**)) and titanyl bearing (TiOPc (**4**)) examples are among the rarely reported MPc compounds, and the performance of these ones are higher than the most of the reported ZnPcs. The different photovoltaic performance may be resulted from the low effective nuclear charge of Pc center cation, which influence the electron density f the Pc ring and the anchoring groups. The high efficiency of DSSC incorporating especially TiOPc (4) and H_2Pc (7) may most probably be due to the low aggregation, high solubility in DMSO and acetonitrile solvents and better directionality of their electronic orbitals in the excited states, which is one of the main factors to provide an efficient electron transfer from the excited dye to the TiO_2 conduction band [55]. Current-voltage (I–V) measurements of DSSCs in Fig. 10 were performed under 1000 W/m^2 - AM 1.5 light intensity by using Science Tech SLB-300A. As shown in this Figure, TiOPc (4), ZnPc (6), and H_2Pc (7) dyes bearing DSSCs show overall power conversion efficiencies close to each other with 2.9%, 3.3%, and 2.2%, respectively, while the CoPc (5) shows relatively low efficiency (1.02%). Although the V_{OC} values of the produced solar cells are very close to each other, the current density (J_{SC}) and FF values of the DSSC using TiOPc (**4**) dye is higher than the using other dyes. To compare with synthesized Pc dyes, N719 used as standard dye in DSSC, and the solar cell efficiency was determined as 9.14% (Fig. S19). While N719 shows the incident photon-to-current efficiency (IPCE) of ca 80% at $\lambda = 535$ nm, TiOPc (4), CoPc (5), ZnPc (6), and H_2Pc (7) dyes on the TiO_2 film shows IPCE values of 68%, 52%, 48%, and 34% at $\lambda = 535$ nm (Fig. 11) respectively. Like higher overall power conversion efficiency, TiOPc (4) and H_2Pc (7) also show higher IPCE than those of CoPc (5) and ZnPc (6).

EIS analysis of DSSCs were performed by using VersaSTAT 3 Potentiostat Galvanostat in 1000 W/m^2 AM 1.5 illumination conditions at room temperature. AC oscillator signal was applied as amplitude of 10 mV. The frequency range was driven from 10 mHz to 1 MHz without bias voltage for all samples. The Nyquist plots of DSSCs in Fig. 12a are fitted into the equivalent circuit which given in inset of Fig. 12. Bode plots of DSSCs were given in Fig. 12b which are used to examine the conductivities of the dyes. The series resistance value (R_S), one of the equivalent circuit parameters obtained from the Nyquist curves, represents the resistance of the FTO layer and is found by determining the start point of the curve. There are two kinetic loops in the Nyquist curves in the high and middle frequency regions. The small loop observed in the high frequency region, represents the resistance of R_{CT1}, which is known to originate from the interface between the I^-/I_3^- redox couple and the Pt counter electrode [55,56]. The large loop in the middle frequency region

Table 3
Equivalent circuit parameters of the DSSCs according to electrochemical impedance spectroscopy.

Dye	R_S(Ω)	R_{CT1}(Ω)	R_{CT2} (Ω)	f_{max} (Hz)	τ_e (ms)	$C_{\mu 2}$ (μF)	τ_n (ms)
TiOPc (4)	10.30	162.1	138.6	348.12	0.46	43.7	6.1
CoPc (5)	127.51	328	583.4	794.33	0.20	132.3	77
ZnPc (6)	118.54	220	420.5	630.96	0.25	82.4	34
H_2Pc (7)	11.46	27.95	360.8	534.28	0.29	52.7	19
N719	9.72	19.07	15.58	196.64	0.81	15.3	0.24

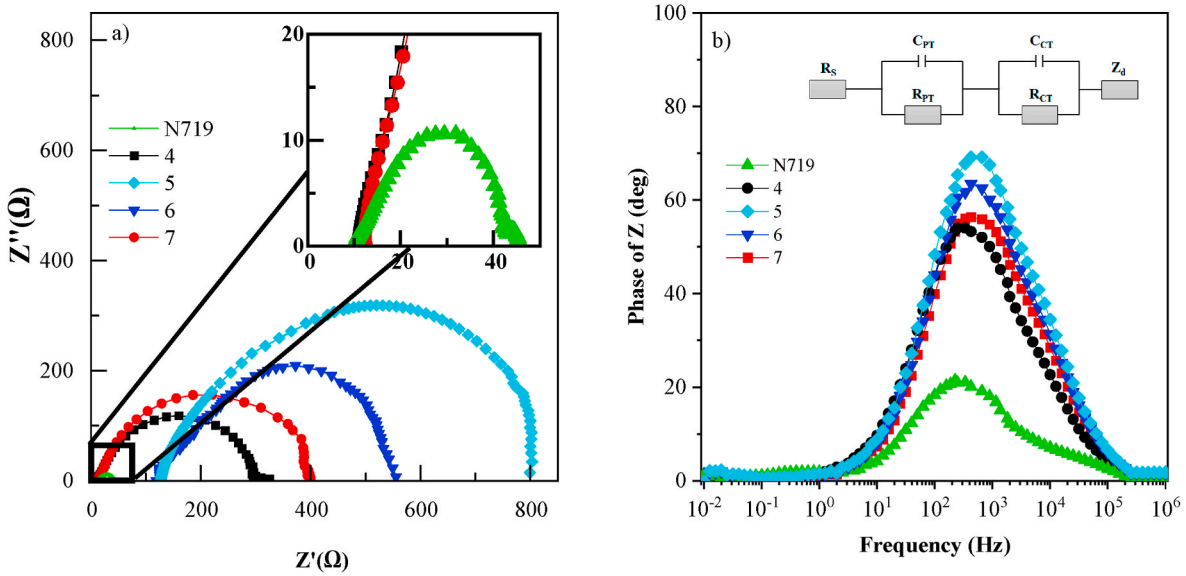

Fig. 12. **a**) Nyquist plots and **b**) Bode plots of the DSSCs based on TiOPc (**4**), CoPc (**5**), ZnPc (**6**), H_2Pc (**7**), and N719.

shows R_{CT2}, which is the charge transfer resistance between TiO_2/Pc sensitizer/I^-/I_3^- redox couple interfaces [57]. Since the TiO_2 semiconductor, I^-/I_3^- redox couple and Pt counter electrode used in the fabrication of the DSSCs are constant in the study, it is expected that the R_{CT2} resistance value in the Nyquist curves will be one-to-one effective on the efficiency, depending on the dye, and it has been observed that this is true when the DSSC efficiencies and the R_{CT2} resistance values are compared. In addition, electron lifetime (τ_e) and electron transport time (τ_n) values were calculated by using the highest frequency (f_{max}) and chemical capacitance ($C_{\mu 2}$) values in the Bode curves by using equations (1) and (2) given below, and these values are shown in Table 3.

$$\tau_e = \frac{1}{2\pi f_{max}} \tag{10}$$

$$\tau_n = R_{CT2} . C_{\mu 2} \tag{11}$$

When the R_{CT2} resistance values were examined, it was seen that the lowest resistance value after N719 was in the TiOPc (**4**) based solar cell. It is well known the efficiency of the solar cells which have low resistance value is relatively higher than the solar cells have high resistance [55,56]. This also explains why solar cell efficiency is higher in TiOPc (**4**) based solar cell than the others. Similarly, electron lifetime values effect the efficiency of the DSSCs and it is expected that the cell with high electron lifetime value will also have high solar cell efficiency. According to all experimental accounts obtained from the produced solar cells, it has been observed that electrochemical parameters such as resistance, electron lifetime and electron transport time are closely related to the solar cell efficiency and are compatible with the experimental results that obtained. TiOPc (**4**) was found to have longer electron lifetime (0.46 ms) and shorter electron transport time (1.2 ms) than the other dyes used solar cells.

4. Conclusion

In conclusion, in this work, the synthesis, characterization and DSSC, electrochemical, spectroelectrochemical applications of peripherally tetra-substituted Ti(IV), Co(II), Zn(II) and free phthalocyanine dyes bearing carboxylic acid groups were reported. Using redox active metal center in the cavity of Pc considerably altered the electrochemical features of the complexes. Using $Ti^{IV}O$ and Co^{II} metal center added extra redox activity to the Pc ligand, which enhanced functionality of these complexes. Especially TiOPc illustrated very complicated electron transfer properties. Tailoring the core of Pc with $Ti^{IV}O$ and Co^{II} metal center will most probably enhance their functionality in various electrochemical fields. Metal free and titanyl phthalocyanines bearing four peripheral carboxyl anchoring groups indicated high power conversing efficiency in DSSCs. Due to the shorter band gap, longer electron lifetime and shorter electron transport time, TiOPc illustrated higher efficiency than that of H_2Pc. The higher performances of TiOPc and H_2Pc than CoPc (5) and ZnPc (6) may be due to the altering the electron density on the Pc ring due to the different effective nuclear charge of the central cation of the Pc rings. Moreover higher performance from the similar example in the literature may be due to the strength of the binding of these compounds to the TiO_2 semiconductor with the help of four anchoring carboxyl groups.

CRediT authorship contribution statement

Gülnur Keser Karaoğlan: Conceptualization, Methodology, Supervision, Synthesis, Characterization, Investigation, Validation, Formal analysis, Data curation, Visualization, Writing – original draft, Revising the manuscript, Critically for important intellectual content. **Arif Hışır:** Synthesis, Characterization, Investigation, Visualization. **Yaren Erdağ Maden:** Visualization, Investigation. **Mücella Özbay Karakuş:** Performed fabrication and applications of dye-sensitized solar cells (DSSCs), Analyzed the data. **Atıf Koca:** Conceptualization, Methodology, Supervision, Investigation, Validation, Formal analysis, Data curation, Visualization, Writing – original draft, Revising the manuscript, Critically for important intellectual content.

Declaration of competing interest

The authors declare that they have no known competing financial interests or personal relationships that could have appeared to influence the work reported in this paper.

Acknowledgments

This work was supported by Yildiz Technical University (Project No. 2016-01-02-DOP03), Marmara University BAPKO (Project No. FYL-2022-10414). Atıf Koca thanks Turkish Academy of Sciences (TUBA) for support.

Appendix A. Supplementary data

Supplementary data to this article can be found online at https://doi.org/10.1016/j.dyepig.2022.110390.

References

[1] Koca A. Copper phthalocyanine complex as electrocatalyst for hydrogen evolution reaction. Electrochem Commun 2009;11:838–41. https://doi.org/10.1016/j.elecom.2009.02.001.
[2] Alsudairi A, Li J, Ramaswamy N, Mukerjee S, Abraham K, Jia Q. Resolving the iron phthalocyanine redox transitions for ORR catalysis in aqueous media. J Phys Chem Lett 2017;8:2881–6. https://doi.org/10.1021/acs.jpclett.7b01126.
[3] Ozoemena KI, Nyokong T. Novel amperometric glucose biosensor based on an ether-linked cobalt (II) phthalocyanine–cobalt (II) tetraphenylporphyrin pentamer as a redox mediator. Electrochim Acta 2006;51:5131–6. http://hdl.handle.net/10962/d1004148.
[4] Mani V, Devasenathipathy R, Chen SM, Huang ST, Vasantha V. Immobilization of glucose oxidase on graphene and cobalt phthalocyanine composite and its application for the determination of glucose. Enzym Microb Technol 2014;66:60–6. https://doi.org/10.1016/j.enzmictec.2014.08.009.
[5] Lin CL, Lee CC, Ho KC. Spectroelectrochemical studies of manganese phthalocyanine thin films for applications in electrochromic devices. J Electroanal Chem 2002;524:81–9. https://doi.org/10.1016/S0022-0728(02)00757-X.
[6] Solis C, Baigorria E, Milanesio ME, Morales G, Durantini EN, Otero L, Gervaldo M. Electrochemical polymerization of EDOT modified Phthalocyanines and their applications as electrochromic materials with green coloration, and strong absorption in the Near-IR. Electrochim Acta 2016;213:594–605. https://doi.org/10.1016/j.electacta.2016.07.086.
[7] Garcia-Iglesias M, Yum JH, Humphry-Baker R, Zakeeruddin SM, Péchy P, Vázquez P, Palomares E, Grätzel M, Nazeeruddin MK, Torres T. Effect of anchoring groups in zinc phthalocyanine on the dye-sensitized solar cell performance and stability. Chem Sci 2011;2:1145–50. https://doi.org/10.1039/C0SC00602E.
[8] Sarker AK, Kang MG, Hong JD. A near-infrared dye for dye-sensitized solar cell: catecholate-functionalized zinc phthalocyanine. Dyes Pigments 2012;92:1160–5. https://doi.org/10.1016/j.dyepig.2011.07.002.
[9] Tunç G, Güzel E, Şişman İ, Ahsen V, Cardenas-Jiron G, Gürek AG. Effect of new asymmetrical Zn (ii) phthalocyanines on the photovoltaic performance of a dye-sensitized solar cell. New J Chem 2019;43:14390–401. https://doi.org/10.1039/C9NJ02585E.
[10] Amao Y, Komori T. Dye-sensitized solar cell using a TiO_2 nanocrystalline film electrode modified by an aluminum phthalocyanine and myristic acid coadsorption layer. Langmuir 2003;19:8872–5. https://doi.org/10.1021/la035001u.
[11] Komori T, Amao Y. Dye-sensitized solar cell with the near-infrared sensitization of aluminum phthalocyanine. J Porphyr Phthalocyanines 2003;7:131–6. https://doi.org/10.1142/S1088424603000185.
[12] Li X, Wang H, Wu H. Phthalocyanines and their analogs applied in dye-sensitized solar cell. In: Mingos DMP, Day P, Duan X, Gade LH, Poeppelmeier KR, Parkin G, Sauvage JP, editors. Functional phthalocyanine molecular materials. Berlin Heidelberg: E-Publishing Inc; Springer-Verlag; 2010. p. 229–73.
[13] Yu L, Fan K, Duan T, Chen X, Li R, Peng T. Efficient panchromatic light harvesting with co-sensitization of zinc phthalocyanine and bithiophene-based organic dye for dye-sensitized solar cells. ACS Sustainable Chem Eng 2014;2:718–25. https://doi.org/10.1021/sc400532g.
[14] Siddique SA, Arshad M, Naveed S, Mehboob MY, Adnan M, Hussain R, Ali B, Siddique MBA, Liu X. Efficient tuning of zinc phthalocyanine-based dyes for dye-sensitized solar cells: a detailed DFT study. RSC Adv 2021;11:27570–82. https://doi.org/10.1039/D1RA04529F.
[15] Harmandar K, Granados-Tavera K, Gezgin M, Nebioğlu M, Şişman İ, Cárdenas-Jirón G, Atilla D, Gürek AG. A new sterically hindered asymmetric zinc phthalocyanine as an efficient sensitizer for dye-sensitized solar cells. New J Chem 2022;46:714–25. https://doi.org/10.1039/D1NJ04441A.

[16] Amao Y, Yamada Y, Aoki K. Preparation and properties of dye-sensitized solar cell using chlorophyll derivative immobilized TiO_2 film electrode. J Photochem Photobiol, A 2004;164:47–51. https://doi.org/10.1016/j.jphotochem.2003.11.011.
[17] Martín-Gomisa L, Barea EM, Fernández-Lázaroa F, Bisquert J, Sastre-Santos Á. Dye sensitized solar cells using non-aggregated silicon phthalocyanines. J Porphyr Phthalocyanines 2011;15:1004–10. https://doi.org/10.1142/S1088424611003914.
[18] Yıldız B, Arslan BS, Güzel E, Nebioğlu M, Menges N, Şişman İ, Şener MK. Non-aggregating zinc phthalocyanine sensitizer with bulky diphenylphenoxy donor groups and pyrazole-3-carboxylic acid anchoring group for coadsorbent-free dye-sensitized solar cells. Sol Energy 2021;226:173–9. https://doi.org/10.1016/j.solener.2021.08.033.
[19] Urbani M, Ragoussi ME, Nazeeruddin MK, Torres T. Phthalocyanines for dye-sensitized solar cells. Coord Chem Rev 2019;381:1–64.
[20] Brogdon P, Cheema H, Delcamp JH. Near-infrared-absorbing metal-free organic, porphyrin, and phthalocyanine sensitizers for panchromatic dye-sensitized solar cells. ChemSusChem 2018;11:86–103. https://doi.org/10.1002/cssc.201701441.
[21] Yasseen FA, Al-Temimei FA. Electronic structures and photovoltaic properties of a novel phthalocyanine and titanium dioxide phthalocyanine for dye sensitized-solar cells. GSCARR 2021;6:107–15. https://doi.org/10.30574/gscarr.2021.6.3.0046.
[22] Palomares E, Martínez-Díaz MV, Haque SA, Torres T, Durrant JR. State selective electron injection in non-aggregated titanium phthalocyanine sensitised nanocrystalline TiO_2 films. Chem Commun 2004;18:2112–3. https://doi.org/10.1039/B407860H.
[23] Dube E, Nwaji N, Oluwole DO, Mack J, Nyokong T. Investigation of photophysicochemical properties of zinc phthalocyanines conjugated to metallic nanoparticles. J Photochem Photobiol, A 2017;349:148–61. https://doi.org/10.1016/j.jphotochem.2017.09.020.
[24] Sevim AM, Arıkan S, Koca A, Gül A. Synthesis and spectroelectrochemistry of new phthalocyanines with ester functionalities. Dyes Pigments 2012;92:1114–21. https://doi.org/10.1016/j.dyepig.2011.07.015.
[25] Karadağ S, Bozoğlu C, Şener MK, Koca A. Synthesis and electrochemical properties of a double-decker lutetium (III) phthalocyanine bearing electropolymerizable substituents on non-peripheral positions. Dyes Pigments 2014;100:168–76. https://doi.org/10.1016/j.dyepig.2013.09.005.
[26] Qu P, Meyer GJ. Proton-controlled electron injection from molecular excited states to the empty states in nanocrystalline TiO_2. Langmuir 2001;17:6720–8. https://doi.org/10.1021/la010939d.
[27] Gumrukcu G, Keser Karaoglan G, Erdogmus A, Gul A, Avciata U. Photophysical, photochemical, and BQ quenching properties of zinc phthalocyanines with fused or interrupted extended conjugation. J Chem 2014:435834. https://doi.org/10.1155/2014/435834. 2014.
[28] Özçeşmeci I, Güney O, Okur AI, Gül A. New phthalocyanines containing bulky electron rich substituents. J Porphyr Phthalocyanines 2009;13:753–9. https://doi.org/10.1142/S1088424609000838.
[29] Wei S, Huang D, Li L, Meng Q. Synthesis and properties of some novel soluble metallophthalocyanines containing the 3-trifluromethylphenyoxy moiety. Dyes Pigments 2003;56:1–6. https://doi.org/10.1016/S0143-7208(02)00104-3.
[30] Arıcı M, Arıcan D, Uğur AL, Erdoğmuş A, Koca A. Electrochemical and spectroelectrochemical characterization of newly synthesized manganese, cobalt, iron and copper phthalocyanines. Electrochim Acta 2013;87:554–66. https://doi.org/10.1016/j.electacta.2012.09.045.
[31] Arslan S, Yilmaz I. Preparation, electrochemical, and spectroelectrochemical characterization of a new water-soluble copper phthalocyanine. Inorg Chem Commun 2007;10:385–8. https://doi.org/10.1016/j.inoche.2006.12.004.
[32] Esenpınar AA, Özkaya AR, Bulut M. Synthesis and electrochemical properties of crown ether functionalized coumarin substituted cobalt and copper phthalocyanines. J Organomet Chem 2011;696:3873–81. https://doi.org/10.1016/j.jorganchem.2011.08.045.
[33] Rollmann LD, Iwamoto RT. Electrochemistry, electron paramagnetic resonance, and visible spectra of cobalt, nickel, copper, and metal-free phthalocyanines in dimethyl sulfoxide. J Am Chem Soc 1968;90:1455–63. https://doi.org/10.1021/ja01008a013.
[34] Sevim AM, Yenilmez HY, Aydemir M, Koca A, Bayır ZA. Synthesis, electrochemical and spectroelectrochemical properties of novel phthalocyanine complexes of manganese, titanium and indium. Electrochim Acta 2014;137:602–15. https://doi.org/10.1016/j.electacta.2014.05.149.
[35] Demirbaş Ü, Akyüz D, Barut B, Bayrak R, Koca A, Kantekin H. Electrochemical and spectroelectrochemical properties of thiadiazole substituted metallo-phthalocyanines. Spectrochim Acta Mol Biomol Spectrosc 2016;153:71–8. https://doi.org/10.1016/j.saa.2015.07.105.
[36] Akyüz D, Keleş T, Biyiklioglu Z, Koca A. Electrochemical pesticide sensors based on electropolymerized metallophthalocyanines. J Electroanal Chem 2017;804:53–63. https://doi.org/10.1016/j.jelechem.2017.09.044.
[37] Demir F, Erdoğmuş A, Koca A. Titanyl phthalocyanines: electrochemical and spectroelectrochemical characterizations and electrochemical metal ion sensor applications of Langmuir films. J Electroanal Chem 2013;703:117–25. https://doi.org/10.1016/j.jelechem.2013.05.012.
[38] Çakır D, Bekircan O, Biyiklioglu Z. 1, 2, 4-Triazole-substituted metallophthalocyanines carrying redox active cobalt (II), manganese (III), titanium (IV) center and their electrochemical studies. Synth Met 2015;201:18–24. https://doi.org/10.1016/j.synthmet.2015.01.006.
[39] Bıyıklıoğlu Z. Novel water soluble and amphiphilic titanium (IV) phthalocyanines and their electrochemical studies. Synth Met 2014;196:48–55. https://doi.org/10.1016/j.synthmet.2014.07.013.
[40] Bıyıklıoğlu Z. Electropolymerizable non-ionic and quaternized ionic titanium (IV) phthalocyanines and their electrochemistry. Dyes Pigments 2013;99:727–32. https://doi.org/10.1016/j.dyepig.2013.07.004.
[41] Arslanoğlu Y, Hayran E, Hamuryudan E. Synthesis, electrochemical and photophysical studies of axially substituted quarternizable titanyl phthalocyanines. Dyes Pigments 2013;97:340–6. https://doi.org/10.1016/j.dyepig.2012.12.022.
[42] He W, Ma C, Chen C, Yu S, Fan Z, Du X, Du G. Synthesis and electrochemical characterization of β-tetra-(2-isopropyl-5-methylphenoxylphthalocyaninato) titanium (IV) Oxide. Russ J Electrochem 2008;44:1466–72. https://doi.org/10.1134/S1023193508120094.
[43] Tau P, Nyokong T. Synthesis, electrochemical and photophysical properties of phthalocyaninato oxotitanium (IV) complexes tetra-substituted at the α and β positions with arylthio groups. Dalton Trans 2006;37:4482–90. https://doi.org/10.1039/B607538J.
[44] Tau P, Nyokong T. Synthesis and electrochemical characterisation of α-and β-tetra-substituted oxo (phthalocyaninato) titanium (IV) complexes. Polyhedron 2006;25:1802–10.
[45] Mbambisa G, Tau P, Antunes E, Nyokong T. Synthesis and electrochemical properties of purple manganese (III) and red titanium (IV) phthalocyanine complexes octa-substituted at non-peripheral positions with pentylthio groups. Polyhedron 2007;26:5355–64. https://doi.org/10.1016/j.poly.2007.08.007.
[46] Sakamoto K, Ohno E. Electrochemical characterization of soluble cobalt phthalocyanine derivatives. Dyes Pigments 1998;37:291–306. https://doi.org/10.1016/S0143-7208(97)00083-1.
[47] Nevin W, Liu W, Melnik M, Lever A. Spectro-electrochemistry of cobalt and iron tetrasulphonated phthalocyanines. J Electroanal Chem 1986;213:217–34. https://doi.org/10.1016/0022-0728(86)80204-2.
[48] Acar ET, Tabakoglu TA, Atilla D, Yuksel F, Atun G. Synthesis, electrochemistry and electrocatalytic activity of cobalt phthalocyanine complexes–effects of substituents for oxygen reduction reaction. Polyhedron 2018;152:114–24. https://doi.org/10.1016/j.poly.2018.06.018.
[49] Akinbulu IA, Nyokong T. Syntheses and investigation of the effects of position and nature of substituent on the spectral, electrochemical and spectroelectrochemical properties of new cobalt phthalocyanine complexes. Polyhedron 2010;29:1257–70.
[50] Obirai J, Nyokong T. Synthesis, spectral and electrochemical characterization of mercaptopyrimidine-substituted cobalt, manganese and Zn (II) phthalocyanine complexes. Electrochim Acta 2005;50:3296–304. https://doi.org/10.1016/j.electacta.2004.12.003.
[51] Ozoemena KI, Nyokong T. Comparative electrochemistry and electrocatalytic activities of cobalt, iron and manganese phthalocyanine complexes axially co-ordinated to mercaptopyridine self-assembled monolayer at gold electrodes. Electrochim Acta 2006;51:2669–77. https://doi.org/10.1016/j.electacta.2005.08.007.
[52] Agboola B, Ozoemena KI, Nyokong T. Synthesis and electrochemical characterisation of benzylmercapto and dodecylmercapto tetra substituted cobalt, iron, and zinc phthalocyanines complexes. Electrochim Acta 2006;51:4379–87. https://doi.org/10.1016/j.electacta.2005.12.017.
[53] Koca A. Spectroelectrochemistry of phthalocyanines. In: Zagal JH, Bedioui F, editors. Electrochemistry of N4 macrocyclic metal complexes. Switzerland: E-Publishing Inc; Springer; 2016. p. 135–200.
[54] Mori S, Nagata M, Nakahata Y, Yasuta K, Goto R, Kimura M, Taya M. Enhancement of incident photon-to-current conversion efficiency for phthalocyanine-sensitized solar cells by 3D molecular structuralization. J Am Chem Soc 2010;132(12):4054–5.
[55] Nazeeruddin MK, Humphry-Baker R, Gratzel M, Wohrle D, Schnurpfci G, Schnesder G, Hirth A, Tronbach N, Nazeeruddin MK, Humphry-Baker R, Grätzel M, Wöhrle D, Schnurpfeil G, Schneider G, Trombach N. Efficient near-IR sensitization of nanocrystalline TiO 2 films by zinc and aluminum phthalocyanines. J Porphyr Phthalocyanines 1999;3:230–7. 1999.
[56] Ilgün C, Sevim AM, Çakar S, Özacar M, Gül A. Novel Co and Zn-Phthalocyanine dyes with octa-carboxylic acid substituents for DSSCs. Sol Energy 2021;218:169–79. https://hdl.handle.net/20.500.12619/95692.
[57] Cakar S, Özacar M. The pH dependent tannic acid and Fe-tannic acid complex dye for dye sensitized solar cell applications. J Photochem Photobiol Chem 2019;371:282–91. https://doi.org/10.1016/j.jphotochem.2018.11.030.
[58] Obirai J, Nyokong T. Synthesis, spectral and electrochemical characterization of mercaptopyrimidine-substituted cobalt, manganese and Zn (II) phthalocyanine complexes. Electrochim Acta 2005;50:3296–304. https://doi.org/10.1016/j.electacta.2004.12.003.
[59] Özen ÜE, Keleş T, Bıyıklıoğlu Z, Koca A, Özkaya AR. Electropolymerization and electrochemical pesticide sensor application of metallophthalocyanines bearing polymerizable morpholin groups. J Electrochem Soc 2016;163:B673–82. https://doi.org/10.1149/2.0241614jes.
[60] Ghazal B, Azizi K, Ewies EF, Youssef AS, Mwalukuku VM, Demadrille R, Torres T, Makhseed S. Push–pull zinc phthalocyanine bearing hexa-tertiary substituted carbazolyl donor groups for dye-sensitized solar cells. Molecules 2020;25(7):1692. https://doi.org/10.3390/molecules25071692.
[61] Sevim AM, Çakar S, Özacar M, Gül A. Electrochemical and photovoltaic properties of highly efficient solar cells with cobalt/zinc phthalocyanine sensitizers. Sol Energy 2018;160:18–24. https://doi.org/10.1016/j.solener.2017.12.001.
[62] Reddy PY, Giribabu L, Lyness C, Snaith HJ, Vijaykumar C, Chandrasekharam M, Lakshmikantam M, Yum JH, Kalyanasundaram K, Grätzel M. Efficient sensitization of nanocrystalline TiO2 films by a near-IR-absorbing unsymmetrical zinc

phthalocyanine. Angew Chem 2007;119:377–80. https://doi.org/10.1002/anie.200603098.

[63] Cid JJ, García-Iglesias M, Yum JH, Forneli A, Albero J, Martínez-Ferrero E, Vázquez P, Grätzel M, Nazeeruddin MK, Palomares E. Structure–function relationships in unsymmetrical zinc phthalocyanines for dye-sensitized solar cells. Chem Eur J 2009;15:5130–7. https://doi.org/10.1002/chem.200801778.

[64] Ghadari R, Sabri A, Saei Ps Kong FT, Marques HM. Phthalocyanine-silver nanoparticle structures for plasmon-enhanced dye-sensitized solar cells. Sol Energy 2020;198:283–94. https://doi.org/10.1016/j.solener.2020.01.053.